Echo Spectroscopy in Multilevel Quantum-Mechanical Rotors

Dina Rosenberg,[1,2] Ran Damari,[1,2] and Sharly Fleischer[1,2,*]
[1]Raymond and Beverly Sackler Faculty of Exact Sciences, School of Chemistry, Tel Aviv University, Tel Aviv 6997801, Israel
[2]Tel-Aviv University center for Light-Matter-Interaction, Tel Aviv 6997801, Israel

(Received 23 July 2018; published 3 December 2018)

We study the dynamics of rotational echoes in gas phase molecular ensembles and their dependence on the delay and intensity of the excitation pulses. We explore the unique dynamics of alignment echoes that arise from the multilevel nature of the molecular rotors and impose severe difficulties in utilizing echo responses for rotational spectroscopy. We show experimentally and theoretically that judicious control of both the delay and intensity of the second pulse enables multilevel "rotational echo spectroscopy." The proposed methodology paves the way to rotational spectroscopy in high-density gas samples.

DOI: 10.1103/PhysRevLett.121.234101

Echo spectroscopy is a widely utilized technique in magnetic-resonance spectroscopy [1], imaging [2], electronic [3–5] and vibrational spectroscopy [6–9] enabling one to experimentally decipher dephasing from decoherence dynamics and determine their rates selectively. Only recently has echo spectroscopy emerged into gas-phase rotational dynamics in a series of works that demonstrated alignment [10] and orientation [11] echoes induced by ultrashort optical and terahertz pulses. In an elegant interplay between the inherently periodic rotational dynamics and the induced echo responses, "fractional echoes" [12], "imaginary echoes" [13], and even "rotated echoes" [14] induced by polarization-skewed pulses were recently demonstrated. Motivated by utilizing alignment echoes for gas-phase rotational spectroscopy, we recently demonstrated the rephasing of centrifugally distorted molecular rotations via alignment echoes (ALECs) in methyl iodide [15] and found that, while they share the basic physics of two-level photon echoes, they substantially differ by several other traits discussed hereafter. In this work, we study the dependence of ALECs on the delay between the two excitation pulses. This dependence is absent from two-level systems and arises from multiple transition pathways that interfere within the multilevel rotational manifold and govern the observed dynamics. We further show that judicious control of the rephasing pulse intensity facilitates multilevel rotational echo spectroscopy and offers additional desirable spectroscopic capabilities, with specific applications to high-density gas samples.

Coherent rotational dynamics.—Laser-induced molecular rotation has been thoroughly explored for more than three decades [16–19]. Since the pioneering works of rotational coherence spectroscopy [20], rotational control became an essential component in various state-of-the-art techniques aiming to extract "molecular frame" spectroscopic signatures (e.g., high-harmonic generation [21–23], ultrafast x-ray diffraction [24], and photoelectron [25] and Coulomb-explosion [26] imaging). In brief, an ultrashort ($\sim$100 fs duration) laser pulse imparts torque to molecular rotors, resulting in their rotation toward the pulse polarization direction (z axis) and their preferred angular distribution along the z axis (alignment). Upon field-free rotation, the rotors dephase and regain their isotropic distribution shortly after. However, due to quantization of angular momentum, the rotational dynamics is inherently periodic and manifest in recurrences of the alignment with each period of the motion, giving rise to a series of alignment events separated by $T_{\mathrm{rev}} = (2B)^{-1}$, termed the "revival period" (B-molecular rotational constant in [Hz] [27,28]). High-density molecular ensembles have a severely limited coherence time due to the fast collision rate; thus they entail a spectroscopic technique that enables the extraction of coherent rotational responses at timescales significantly shorter than T_{rev}.

Echo spectroscopy in two-level systems.—A typical photon-echo experiment includes two time-delayed pulses. The first (with a $\pi/2$ area) induces a coherent superposition of the two levels followed by field-free evolution for time $\Delta\tau$ (delay between the pulses termed "waiting time"), during which the system experiences dephasing and decoherence that manifest by signal decay. At $t = \Delta\tau$, the second pulse (with an area of π) is applied to effectively reverse the time evolution such that after another period of free evolution, at $t = 2\Delta\tau$, the system is "in phase" again and an echo signal is observed [1]. By repeating the experiment with varying $\Delta\tau$, the decoherence rate is selectively extracted. However, the abovementioned scheme requires that *the echo response is independent of* $\Delta\tau$. While this condition is inherently satisfied in two-level systems (even for pulses other than $\pi/2$ and π, respectively [29]), it does not hold in multilevel rotational systems explored in this work.

Experiment.—The rotational dynamics of carbonyl sulfide (OCS) was measured via the weak-field polarization

detection technique [10,30–32] as reported previously [15,33,34]. The setup consists of two pump pulses ($\lambda = 800$ nm, 100 fs duration) with controlled delay apart and a probe beam ($\lambda = 400$ nm, with a computer-controlled delay). The pump and probe beams cross at their Rayleigh range inside the sample cell at a small angle. As will become clearer later in the text, this geometry is crucial for our experiment. The pump pulses' energies are varied selectively via two attenuators and, in what follows, are reported in [mW] such that 1 mW corresponds to 2 μJ (per pulse) with an intensity of 5×10^{12} W/cm^2 at the focus. The ALEC response manifests as a transient optical birefringence and is detected by the change in the probe polarization [35]. The observed signal is proportional to the change in the degree of alignment $\Delta I/I(t) \propto [\cos^2\theta_{(t)} - 1/3]$ with θ the angle between the molecular axis and the z axis [33,36,37].

Figure 1 depicts the simulated [Fig. 1(b)] and experimental [Fig. 1(c)] ALEC amplitudes as a function of the delay ($\Delta\tau$) between two pulses with fixed intensities ($P_1 = 9.2$ mW and $P_2 = 4.2$ mW). We quantify the ALEC amplitude by its peak-to-peak difference [marked S_{echo} in Fig. 1(a)] [15]. For example, the "$*$" in Fig. 1(b) marks the echo induced by two pulses with a delay $\tau = 0.07T_{\text{rev}}$ apart and its amplitude S_{echo}, observed at $t = 2\Delta\tau = 0.14T_{\text{rev}}$. We find a fairly parabolic dependence of S_{echo} on $\Delta\tau$ in each quadrant of T_{rev}, in agreement with the experimental results in Fig. 1(c), where S_{echo} vs $\Delta\tau$ was measured at the first quadrant [$0 < \Delta\tau < 0.25T_{\text{rev}}$]. From Figs. 1(b) and 1(c), one sees that the most efficient ALEC response (maximal S_{echo} amplitude) is induced with $\Delta\tau = 1/8T_{\text{rev}}$ ($3/8$, $5/8$, $7/8T_{\text{rev}}$). In what follows, we show that this dependency results from interferences of multiple coherent pathways within the rotational-state manifold. While it is common to represent coherent pathways by double-sided Feynman diagrams [11,15,38], we believe that their interferences are better conveyed in the following two-dimensional representation, inspired by the rotational-density matrix (RDM).

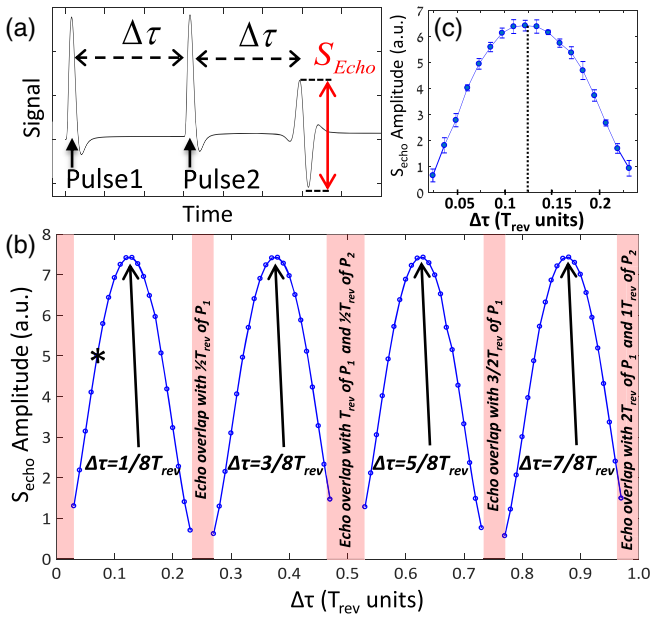

FIG. 1. (a) Simulated rotational response induced by two laser pulses (pulse 1 and pulse 2, respectively) with a delay $\Delta\tau$ apart. The echo signal is observed at $t = 2\Delta\tau$ and its amplitude given by the peak-to-peak difference (marked S_{echo}). (b) Simulated S_{echo} as a function of $\Delta\tau$ (in units of T_{rev}). The pulses' intensities are fixed. (c) Experimental data for the first quadrant $0 < \Delta\tau < T$ measured in OCS gas sample ($T_{\text{rev}} = 82$ ps, 85 torr, room temperature).

Theoretical model.—All of the theoretical simulations in this work were performed by numerically propagating the RDM using the Liouville–von Neumann equation $\partial\hat{\rho}/\partial t = -i/\hbar[\hat{H}, \hat{\rho}]$, with $\hat{H} = \hat{L}^2/2I - \frac{1}{4}\Delta\alpha|E_{(t)}|^2\cos^2\theta$. ($\hat{L}$, angular momentum operator; I, moment of inertia; $\Delta\alpha$, anisotropic molecular polarizability; $|E_{(t)}|^2$, pulse envelope; and θ, the polar angle) (see [35] for details). Linear molecules are typically modeled as quantum-mechanical rigid rotors [17], with eigenstates $|J, m\rangle$ (spherical-harmonic functions) and eigenenergies $E_J = BJ(J+1)$. We choose the quantization axis of the rotors along the polarization axis of the pump pulses for convenience ($\hat{z}$). With this setting, only transitions with $\Delta m = 0$ and $\Delta J = \pm 2$ are allowed. Thus, we can restrict the discussion to the J quantum number solely. In Fig. 2, we consider only ALEC responses induced via one and two Raman interactions with the first (P_1) and second (P_2) pulses, respectively (i.e., $S_{\text{echo}} \propto P_1$, P_2^2 as found in Ref. [15]). The P_1-induced transition is depicted

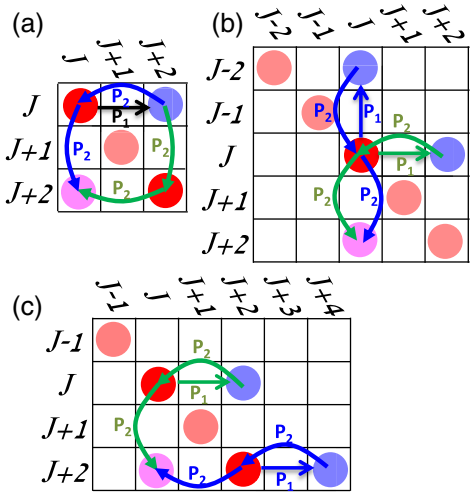

FIG. 2. Pictorial RDM representations of (a) an effective two-level system invoked by the Raman selection rule ($\Delta J = \pm 2$). (b) Two coherent pathways starting from a mutual population term $|J\rangle\langle J|$ and interfere to create the rephasing coherence term $|J+2\rangle\langle J|$. (c) Two coherent pathways starting from two neighboring population terms $|J\rangle\langle J|$ and $|J+2\rangle\langle J+2|$ that interfere at the rephasing coherence term $|J+2\rangle\langle J|$.

by a straight arrow and P_2-induced transitions by (two) curved arrows. At $t < 0$ (before the first laser interaction), the system is described by a set of (thermal) population terms, represented by the bright-red dots along the diagonal of the RDMs (the pale-red terms do not participate in scenarios described hereafter).

The 3×3 RDM in Fig. 2(a) is an effective two-level system, since both interacting pulses do not couple $J+1$ to its neighboring states ($\Delta J = \pm 2$). At $t = 0$, P_1 (black arrow) induces the $|J\rangle\langle J+2|$ coherence (blue dot, second off-diagonal) which governs the alignment dynamics [38]. During the waiting time ($0 < t < \Delta\tau$), the $|J\rangle\langle J+2|$ coherence accumulates phase: $\exp(-i\phi_{|J\rangle\langle J+2|}) = \exp[-i(E_{J+2} - E_J)\Delta\tau/\hbar]$. Next, P_2 is applied ($t = \Delta\tau$) and interacts with $|J\rangle\langle J+2|$ via two Raman transitions to create the conjugate coherence term $|J+2\rangle\langle J|$—the latter accumulates phase at the exact same frequency but with a negative sign: $\exp(-i\phi_{|J+2\rangle\langle J|}) = \exp[-i(E_J - E_{J+2})\Delta\tau/\hbar]$; hence, at $t = \Delta\tau$, the total phase accumulated is $\phi_{|J\rangle\langle J+2|} + \phi_{|J+2\rangle\langle J|} = 0$, and a fully rephased echo is observed. In fact, even for the two-level case, there are two interfering pathways (blue and green curved arrows). However, since both pathways share the $|J\rangle\langle J+2|$ coherence term, they accumulate the exact same phase, $\exp(-i\phi_{|J\rangle\langle J+2|})$, and their phase difference remains zero for all $\Delta\tau$'s—i.e., their interference at $|J+2\rangle\langle J|$ is independent of $\Delta\tau$ (and so is the echo amplitude).

In our multilevel rotational system, those pathways exceed beyond the 2×2 space of two-level systems and accumulate phase difference (for different $\Delta\tau$) that results in the dependence of the ALEC on $\Delta\tau$ [Figs. 1(b) and 1(c)]. Figures 2(b) and 2(c) are exemplary cases where different pathways start at the same initial population term or at adjacent terms, respectively.

Case 1: Same population term [Fig. 2(b)].—Consider $|J\rangle\langle J|$ as the initial population term. P_1 provides one Raman interaction to create both the $|J-2\rangle\langle J|$ and $|J\rangle\langle J+2|$ (blue and green P_1 arrows) that accumulate phase as $\exp(-i\Phi_{|J-2\rangle\langle J|}) = \exp[-i(E_J - E_{J-2})\Delta\tau/\hbar]$ and $\exp(-i\phi_{|J\rangle\langle J+2|}) = \exp[-i(E_{J+2} - E_J)\Delta\tau/\hbar]$, respectively. Their interference at the final rephasing term depends on their phase difference $\Delta\phi = \phi_{|J\rangle\langle J+2|} - \phi_{|J-2\rangle\langle J|} = [(E_{J+2} - E_J) - (E_J - E_{J-2})]\Delta\tau/\hbar = 8B\Delta\tau/\hbar$. Thus, by setting $\Delta\tau = h/16B = 1/8T_{\mathrm{rev}}$ (or $3/8, 5/8, 7/8T_{\mathrm{rev}}$) in units of the revival period ($T_{\mathrm{rev}} = h/2B$), the two pathways accumulate $\pi(3\pi, 5\pi, 7\pi)$, respectively, phase apart and *constructively interfere* to create the maximal rephasing coherence $|J+2\rangle\langle J|$ and the largest S_{echo} as shown in Fig. 1. In accordance, for $\Delta\tau = 2/8, 4/8, 6/8T_{\mathrm{rev}}$, the two pathways accumulate $2\pi, 4\pi, 6\pi$ difference in phase, that minimizes the S_{echo} due to destructive interference. In conclusion, these two pathways are deemed to interfere destructively, unless a phase difference (optimally π) is introduced between them by setting $\Delta\tau$ to $[(2n+1)/8]T_{\mathrm{rev}}(n \in 0, \mathbb{N})$.

Case 2: Two adjacent population terms [Fig. 2(c)].—Interfering pathways may originate from different initial population terms $|J\rangle\langle J|$ and $|J+2\rangle\langle J+2|$ as exemplified in Fig. 2(c). While the two pathways marked by the green and blue arrows start as incoherent, their induced transitions interfere at the $|J+2\rangle\langle J|$ coherence (pink dot). Whether it is constructive or destructive depends on their phase difference as in case 1: $\Delta\phi = \phi_{|J\rangle\langle J+2|} - \phi_{|J+2\rangle\langle J+4|} = 8B\Delta\tau/\hbar$.

Figure 2 considers the lowest number of interactions needed for inducing ALECs. However, higher numbers of interactions (e.g., two and three interactions with P_1 and P_2, respectively) also contribute and are accounted for by our simulations [35] and their ramifications are discussed hereafter.

ALEC dependence on both $\Delta\tau$ and P_2.—As P_1 and P_2 intensities increase, multiple light-molecule interactions gradually alter the dependence of S_{echo} on the pump pulses' intensities. While the linear dependence of S_{echo} on P_1 is retained, its quadratic dependence on P_2 evolves into an oscillatory dependence, the initial (low P_2 intensities) region of which can be fitted by a sinusoidal squared function as reported previously [15]. With even higher P_2 intensities, S_{echo} is found to oscillate and gradually decay.

Figure 3(a) depicts simulation results of S_{echo} vs P_2 for different delays $\Delta\tau = (0.04, 0.06, 0.08, 0.125T_{\mathrm{rev}})$, showing a decaying oscillatory behavior of S_{echo} as P_2 increases. Negative S_{echo} values correspond to phase-inverted ALECs, shown in Fig. 3(a) (green ALEC transients). This phase inversion is yet another indication for multiple light-matter interactions that become effective at increased P_2 intensities; however, they remain beyond the scope of this work. Thus, we restrict our discussion to the lower P_2 region, where S_{echo} can be fitted by $S_{\mathrm{echo}} = a\sin^2(bP_2)$ and where strong-field effects such as ionization are experimentally avoided. Figure 3(b) shows experimental results of S_{echo} vs P_2 with fixed $\Delta\tau = 1/8T_{\mathrm{rev}}$ for three P_1 values: 6, 7.5, and 9.8 mW (12, 15, and 19.6 μJ/pulse, respectively). The insets depict the normalized experimental data and the linear dependence [15] of S_{echo} on P_1, verifying that *the modulation of S_{echo} with P_2 is decoupled from P_1 intensity.* Figure 3(c) depicts the experimentally measured S_{echo} vs $\Delta\tau$ (in the range $0 < \Delta\tau < 1/4T_{\mathrm{rev}}$) for a fixed $P_1 =$ 9.2 mW and five different P_2 values (4.2 [blue], 6.6 [red], 8.25 [green], 10 [yellow], and 12.3 mW [black]). Different P_2 intensities yield significantly different S_{echo} progressions as readily observed in Fig. 3(c). For low P_2 intensities ($P_2 \leq 4.2$ mW, blue data), S_{echo} peaks at $\Delta\tau = 1/8T_{\mathrm{rev}}$ with parabolic progression similar to Figs. 1(b) and 1(c). With $P_2 \geq 6.2$ mW (the other four curves), the maximal S_{echo} amplitudes are found at $\Delta\tau$'s other than $1/8T_{\mathrm{rev}}$. This is consistent with the oscillatory S_{echo} dependence on P_2 shown in Fig. 3(a), where for $P_2 < 30$ (in the arbitrary units of the simulation) the maximal S_{echo} amplitude is always found at

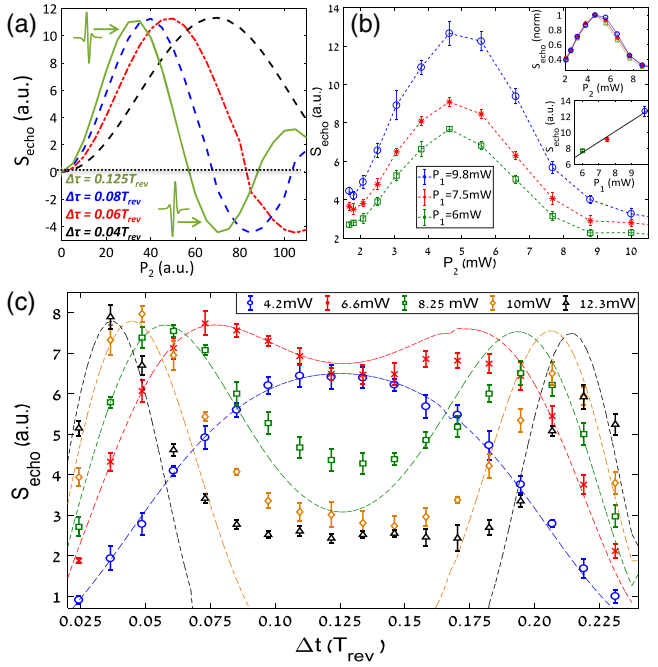

FIG. 3. (a) Simulated results for S_{echo} as a function of P_2 [with constant $P_1 = 20$ (a.u.)] for four delays between pulses (color coded). Simulated echo signals are depicted by the green transients (with inversed phases). (b) Experimental S_{echo} as a function of P_2 (mW) for three P_1 values (color coded) in OCS gas with fixed $\Delta\tau = 1/8T_{rev}$ (=10.28 ps in OCS). Upper inset, the same data only normalized; lower inset, maximal S_{echo} responses (with $P_2 = 4.63$ mW) for the three P_1 intensities—showing the linear dependence of S_{echo} on P_1. (c) Experimental S_{echo} vs $\Delta\tau$ at the first quadrant of the revival period for five different P_2 intensities (color coded in the legend), with a fixed $P_1 = 9.2$ mW. The dashed lines are simulated results with the same color coding.

$\Delta\tau = 1/8T_{rev}$, while for $P_2 > 30$ the $\Delta\tau$ for which maximal S_{echo} is induced gradually shifts to $\Delta\tau < 1/8T_{rev}$ and to $\Delta\tau > 1/8T_{rev}$ symmetrically. The dashed lines are simulated results (color-coded) and capture the experimental trends well, however with better agreement for the low P_2 intensities (blue, red, and green) than for high ones (orange and black). The key reason (in addition to collisional-decoherence effects that are discarded in our simulations) for this discrepancy is the inevitable averaging over the (Gaussian) intensity distribution of the pump pulses by the probe: It is the variation in P_2 intensities experienced by molecules positioned at different locations within the interaction volume that results in a variety of echo amplitudes and even phase reversals [Fig. 3(a)]—all averaged over by the probe beam. As P_2 increases, so does the intensity distribution and corresponding averaging that leads to a larger discrepancy (orange and black data sets). While this averaging is partially reduced by the crossed-beams geometry, the position-dependent ALEC within the interaction volume remains mostly hindered.

Up to now, we have studied the intricate dependence of the rotational echo on P_1, P_2, and $\Delta\tau$. Unlike two-level systems where those three "experimental knobs" are fully decoupled, in our multilevel system P_2 and $\Delta\tau$ are interweaved and result in the convoluted ALEC response shown in Fig. 3. The cross-dependence of S_{echo} on both P_2 and $\Delta\tau$ *obstructs* conventional applications of echo spectroscopy in multilevel rotational systems, such as the selective characterization of decay and decoherence dynamics—a key feature of echo spectroscopy. One possibility is to restrict the examination of S_{echo} to $\Delta\tau$'s that are synced with the revival period ($\Delta\tau + nT_{rev}$, $n \in \mathbb{N}$); however, this approach is severely limited by the decay and decoherence rates, i.e., to samples of sufficiently low densities. Comparing to numerical simulation results like those of Figs. 1 and 3 is yet another option but requires an exact knowledge of the system's dynamics such as the dependence of collisions on the J, m quantum numbers [39].

In what follows, we propose and demonstrate a procedure that overcomes the abovementioned restrictions and enables rotational-echo spectroscopy. The strategy relies on the finding that *the maximal obtainable ALEC* (S^{max}_{echo}) *is dictated solely by* P_1 (and gas parameters $-B$, $\Delta\alpha$, and temperature). This is readily observed in Fig. 3(a), where the maximal S_{echo} amplitudes of all four curves, differing by their $\Delta\tau$, peak at the same value (~11 in the arbitrary units of the simulation). The latter was confirmed by additional decay- and decoherence- free simulations that yielded the same S^{max}_{echo} with up to 1%–2% variation across the $0.02T_{rev} < \Delta\tau < 0.23T_{rev}$ region. Thus, P_1 imparts coherences that are partially rephased by P_2, but the degree

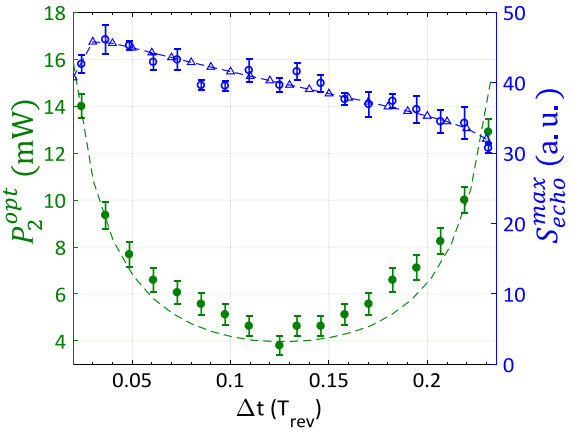

FIG. 4. Experimental results of the maximal echo amplitude (S^{max}_{echo}, marked by blue circles), obtained at various delays between pulses, and the corresponding optimal P_2 intensities (P_2^{opt}, green dots) required to induce them. Theoretical simulations of S^{max}_{echo} and of P_2^{opt} are depicted by the blue triangles (connected by blue dashed curve) and by the green curve, respectively [40]. Note that the x axis depicts the time of the second pulse ($\Delta\tau$) and, thus, the echo signals (with their maximal amplitudes marked by the blue circles) are observed at $2\Delta\tau$.

to which they are rephasable ($S_{\mathrm{echo}}^{\mathrm{max}}$) is independent of the delay $\Delta\tau$ by properly choosing P_2 intensity as demonstrated hereafter.

Figure 4 depicts our experimental (green points, blue circles) and simulated (dashed green and blue curves) results of $S_{\mathrm{echo}}^{\mathrm{max}}$ vs $\Delta\tau$ with fixed P_1 (9.2 mW). For each delay, we have monitored the S_{echo} amplitudes induced by a range of P_2 intensities and recorded $S_{\mathrm{echo}}^{\mathrm{max}}$ and the intensity of P_2 that yielded it (green points, termed P_2^{opt}). We find a minimal P_2^{opt} intensity at $\Delta\tau = 1/8T_{\mathrm{rev}}$—consistent with the analysis of Fig. 2 and in agreement with the simulation results (green dashed curve). The experimental $S_{\mathrm{echo}}^{\mathrm{max}}$ amplitudes (blue circles) show a gradual decay with $\Delta\tau$ due to collisional-decoherence of the OCS gas ensemble (85 torr, room temperature) [33]. Thus, by fitting the experimental $S_{\mathrm{echo}}^{\mathrm{max}}$ to an exponent, one can extract the collisional decoherence of the gas selectively. The dashed blue curve (and blue triangles) depicts our simulated results, multiplied by a decaying exponent to fit the experimental results [40].

Discussion.—We have shown that multilevel rotational systems invoke intricate dynamics that arise from interference among multiple quantum pathways. For rotational-echo spectroscopy, those interferences manifest by inherent coupling of the delay between pulses and the intensity of the second pulse. We have found that, for each $\Delta\tau$, there is a P_2 intensity for which a maximal echo response is induced. Moreover, the amplitude of $S_{\mathrm{echo}}^{\mathrm{max}}$ is independent of $\Delta\tau$, providing an inclusive "experimental anchor" that is easily extracted by varying P_2 intensity and monitoring S_{echo} for a fixed delay between pulses. Then, by varying $\Delta\tau$ and recording $S_{\mathrm{echo}}^{\mathrm{max}}$, one is able to monitor the decay of $S_{\mathrm{echo}}^{\mathrm{max}}$ and extracts the desirable decoherence rate. Here we deliberately experimented with low-density gas samples in order to minimize the collision rates and retain the focus on the basic physics of rotational echoes. However, the strength of the method is in its applicability to dense gas ensembles. The dynamics of such ensembles, governed by the (high) collision rates, are experimentally inaccessible by the conventional rotational coherence spectroscopy due to lifetimes that may be shorter than a revival period, much like in the liquid phase. The proposed scheme is practically decoupled from the revival period and therefore applicable to high-density ensembles. The ability for experimentally identifying the 1/8th revival period (Fig. 4) provides yet another advantage with specific implications to large molecules with very long T_{rev} and is underway in our lab.

We acknowledge Professor Jean-Michel Hartmann and Professor Olivier Faucher for their important remarks and the support of the Israel Science Foundation (ISF) Grants No. 1065/14 and No. 926/18, ISF Grant No. 2797/11 (INREP—Israel National Research Center for Electrochemical Propulsion) and the Wolfson Foundation Grants No. PR/ec/20419 and No. PR/eh/21797

*Corresponding author.
sharlyf@post.tau.ac.il

[1] E. L. Hahn, Phys. Rev. **80**, 580 (1950).
[2] R. Damadian, Science **171**, 1151 (1971).
[3] V. I. Prokhorenko, A. Halpin, and R. J. D. Miller, Opt. Express **17**, 9764 (2009).
[4] R. Inaba, K. Tominaga, M. Tasumi, K. A. Nelson, and K. Yoshihara, Chem. Phys. Lett. **211**, 183 (1993).
[5] J. D. Hybl, A. W. Albrecht, S. M. Gallagher Faeder, and D. M. Jonas, Chem. Phys. Lett. **297**, 307 (1998).
[6] A. Shalit, S. Ahmed, J. Savolainen, and P. Hamm, Nat. Chem. **9**, 273 (2017).
[7] S. Park, K. Kwak, and M. D. Fayer, Laser Phys. Lett. **4**, 704 (2007).
[8] K. A. Merchant, D. E. Thompson, and M. D. Fayer, Phys. Rev. Lett. **86**, 3899 (2001).
[9] D. Zimdars, A. Tokmakoff, S. Chen, S. R. Greenfield, M. D. Fayer, T. I. Smith, and H. A. Schwettman, Phys. Rev. Lett. **70**, 2718 (1993).
[10] G. Karras, E. Hertz, F. Billard, B. Lavorel, J. M. Hartmann, O. Faucher, E. Gershnabel, Y. Prior, and I. S. Averbukh, Phys. Rev. Lett. **114**, 153601 (2015).
[11] J. Lu, Y. Zhang, H. Y. Hwang, B. K. Ofori-Okai, S. Fleischer, and K. A. Nelson, Proc. Natl. Acad. Sci. U.S.A. **113**, 11800 (2016).
[12] G. Karras, E. Hertz, F. Billard, B. Lavorel, G. Siour, J. M. Hartmann, O. Faucher, E. Gershnabel, Y. Prior, and I. S. Averbukh, Phys. Rev. A **94**, 033404 (2016).
[13] K. Lin, P. Lu, J. Ma, X. Gong, Q. Song, Q. Ji, W. Zhang, H. Zeng, J. Wu, G. Karras, G. Siour, J.-M. Hartmann, O. Faucher, E. Gershnabel, Y. Prior, and I. S. H. Averbukh, Phys. Rev. X **6**, 041056 (2016).
[14] K. Lin, J. Ma, X. Gong, Q. Song, Q. Ji, W. Zhang, H. Li, P. Lu, H. Li, H. Zeng, J. Wu, J.-M. Hartmann, O. Faucher, E. Gershnabel, Y. Prior, and I. S. Averbukh, Opt. Express **25**, 24917 (2017).
[15] D. Rosenberg, R. Damari, S. Kallush, and S. Fleischer, J. Phys. Chem. Lett. **8**, 5128 (2017).
[16] H. Stapelfeldt and T. Seideman, Rev. Mod. Phys. **75**, 543 (2003).
[17] S. Fleischer, Y. Khodorkovsky, E. Gershnabel, Y. Prior, and I. S. Averbukh, Isr. J. Chem. **52**, 414 (2012).
[18] M. Lemeshko, R. V. Krems, J. M. Doyle, and S. Kais, Mol. Phys. **111**, 1648 (2013).
[19] Y. Ohshima and H. Hasegawa, Int. Rev. Phys. Chem. **29**, 619 (2010).
[20] P. M. Felker, J. S. Baskin, and A. H. Zewail, J. Phys. Chem. **90**, 724 (1986).
[21] L. S. Spector, M. Artamonov, S. Miyabe, T. Martinez, T. Seideman, M. Guehr, and P. H. Bucksbaum, Nat. Commun. **5**, 3190 (2014).
[22] S. Haessler, J. Caillat, W. Boutu, C. Giovanetti-Teixeira, T. Ruchon, T. Auguste, Z. Diveki, P. Breger, A. Maquet, B. Carré, R. Taïeb, and P. Salières, Nat. Phys. **6**, 200 (2010).
[23] J. Itatani, J. Levesque, D. Zeidler, H. Niikura, H. Pépin, J. C. Kieffer, P. B. Corkum, and D. M. Villeneuve, Nature (London) **432**, 867 (2004).
[24] J. Küpper *et al.*, Phys. Rev. Lett. **112**, 083002 (2014).
[25] C. Z. Bisgaard, O. J. Clarkin, G. Wu, A. M. D. Lee, O. Gessner, C. C. Hayden, and A. Stolow, Science **323**, 1464 (2009).

[26] K. F. Lee, D. M. Villeneuve, P. B. Corkum, A. Stolow, and J. G. Underwood, Phys. Rev. Lett. **97**, 173001 (2006).
[27] T. Seideman, Phys. Rev. Lett. **83**, 4971 (1999).
[28] I. S. Averbukh and N. F. Perelman, Phys. Lett. A **139**, 449 (1989).
[29] J. Hennig, Concepts Magn. Reson. **3**, 125 (1991).
[30] V. Renard, M. Renard, A. Rouzee, S. Guerin, H. R. Jauslin, B. Lavorel, and O. Faucher, Phys. Rev. A **70**, 033420 (2004).
[31] B. Lavorel, O. Faucher, M. Morgen, and R. Chaux, J. Raman Spectrosc. **31**, 77 (2000).
[32] V. Renard, M. Renard, S. Guérin, Y. T. Pashayan, B. Lavorel, O. Faucher, and H. R. Jauslin, Phys. Rev. Lett. **90**, 153601 (2003).
[33] R. Damari, D. Rosenberg, and S. Fleischer, Phys. Rev. Lett. **119**, 033002 (2017).
[34] R. Damari, S. Kallush, and S. Fleischer, Phys. Rev. Lett. **117**, 103001 (2016).
[35] See Supplemental Material at http://link.aps.org/supplemental/10.1103/PhysRevLett.121.234101 for the description of the experimental system and simulation details.
[36] I. F. Tenney, M. Artamonov, T. Seideman, and P. H. Bucksbaum, Phys. Rev. A **93**, 013421 (2016).
[37] P. Peng, Y. Bai, N. Li, and P. Liu, AIP Adv. **5**, 127205 (2015).
[38] S. Fleischer, R. W. Field, and K. A. Nelson, Phys. Rev. Lett. **109**, 123603 (2012).
[39] T. Vieillard, F. Chaussard, F. Billard, D. Sugny, O. Faucher, S. Ivanov, J.-M. Hartmann, C. Boulet, and B. Lavorel, Phys. Rev. A **87**, 023409 (2013).
[40] We fitted the (decay-free) simulated $S_{\mathrm{echo}}^{\mathrm{max}}$ to the experimental results by including an exponential decay rate of $8 \times 10^{-3}\mathrm{ps}^{-1}$ (accounting for OCS revival period 82 ps and the exact time of appearance of S_{echo} at $2 \times \Delta\tau$). We note that the ~125 ps time scale for the echo decay is different from that found for the fundamental revival signals in our previous work [32] and may be the result of some interesting physics that is yet to be explained. The different beam configurations used in the two works: crossing beams (in this work) vs collinear pump-probe configuration (in Ref. [32]) and the different quantification method of the signal amplitude: peak-to-peak amplitude (in this work) vs signal area (in Ref. [32]), respectively, may also contribute to the difference in the extracted decay rates. We note that in this work we deliberately used low gas pressure in order to minimize the collisional decoherence rate at the cost of signal to noise ratio. However, for high gas-pressures (where the proposed scheme may be the only possible method for extracting the decay rate) we expect better signal to noise ratio and correspondingly better accuracy of the extracted decay rates.